10006 *Biochemistry* **2010,** *49,* 10006–10012
DOI: 10.1021/bi101423j

BIOCHEMISTRY
including biophysical chemistry & molecular biology
Article

Comparative Features of Copper ATPases ATP7A and ATP7B Heterologously Expressed in COS-1 Cells†

Yueyong Liu, Rajendra Pilankatta, Yuta Hatori, David Lewis, and Giuseppe Inesi*

California Pacific Medical Center Research Institute, San Francisco, California 94107, United States

Received September 2, 2010; Revised Manuscript Received October 18, 2010

ABSTRACT: ATP7A and ATP7B are P-type ATPases required for copper homeostasis and involved in the etiology of Menkes and Wilson diseases. We used heterologous expression of ATP7A or ATP7B in COS-1 cells infected with adenovirus vectors to characterize differential features pertinent to each protein expressed in the same mammalian cell type, rather than to extrinsic factors related to different cells sustaining expression. Electrophoretic analysis of the expressed protein, before and after purification, prior or subsequent to treatment with endoglycosidase, and evidenced by protein or glycoprotein staining as well as Western blotting, indicates that the ATP7A protein is glycosylated while ATP7B is not. This is consistent with the prevalence of glycosylation motifs in the ATP7A sequence, and not in ATP7B. ATP7A and ATP7B undergo copper-dependent phosphorylation by utilization of ATP, forming equal levels of an "alkali labile" phosphoenzyme intermediate that undergoes similar catalytic (P-type ATPase) turnover in both enzymes. In addition, incubation with ATP yields an "alkali stable" phosphoprotein fraction, attributed to phosphorylation of serines. Alkali stable phosphorylation occurs at lower levels in ATP7A, consistent with a different distribution of serines in the amino acid sequence. Immunostaining of COS-1 cells sustaining heterologous expression shows initial association of both ATP7A and ATP7B with Golgi and the trans-Golgi network. However, in the presence of added copper, ATP7A undergoes prevalent association with the plasma membrane while ATP7B exhibits intense trafficking with cytosolic vesicles. Glycosylation of ATP7A and phosphorylation of ATP7B apparently contribute to their different trafficking and membrane association when expressed in the same cell type.

The human copper ATPases ATP7A and ATP7B sustain essential roles in copper homeostasis, including intracellular copper delivery for inclusion in metalloproteins, membrane trafficking, and export of excess copper from cells (*1*). The catalytic mechanism and related structural features of both ATP7A and ATP7B are similar to those of P-ATPases (*2*), which are members of the acid dehalogenase superfamily (*3*). The mechanism of P-ATPases is based on the presence of transmembrane segments with a binding site (TMBS)[1] for the metal undergoing active transport, and a headpiece that protrudes from the membrane. In analogy to other P-type ATPases, the headpiece of ATP7A and ATP7B includes an N domain with the ATP binding site, a P domain with an aspartyl residue undergoing phosphorylation as an intermediate step in the catalytic cycle, and an A domain containing the conserved TGE motif required for catalytic assistance of the final hydrolytic reaction. A specific feature of mammalian copper ATPases is an amino-terminal extension (NMBD) that includes six copper binding sites in addition to the TMBS (*1*). This N-terminal extension is involved in interactions with chaperone proteins (*4*) and undergoes copper-induced and functionally relevant conformational effects (*5*), which are required for mammalian copper homeostasis.

Much progress in the characterization of ATP7A (Menkes disease protein) and ATP7B (Wilson disease protein) was realized by heterologous expression in insect cells (*6*, *7*), including demonstration of a phosphorylated enzyme intermediate formed by utilization of ATP. Furthermore, an important feature of ATP7B is the presence of serine residues undergoing phosphorylation and possibly involved in functionally relevant interactions (*6*).

ATP7A and ATP7B exhibit trafficking patterns that are likely to be relevant to their functions. Following initial localization in the trans-Golgi network (*8*), the two proteins undergo specific targeting in response to copper. The ATP7A protein is directed to the basolateral membrane in polarized cells (*9*, *10*), while ATP7B was shown to be associated with cytosolic vesicles (*11*) and to target the apical membrane in hepatoma cells (*12*). It is possible that post-translational modification may influence specific trafficking (*13*, *14*), but the extent to which intrinsic features of the two proteins, or different cell types sustaining expression, are responsible for different trafficking patterns is not clear.

With the experiments reported here, we have obtained heterologous expression of ATP7A and ATP7B in the same mammalian cell line (COS-1) infected with adenovirus vectors and characterized features pertinent to each protein expressed in the same cell type, in a manner independent of extrinsic factors

†This work was supported by National Institutes of Health Grant RO1-69830.

*To whom correspondence should be addressed: CPMCRI, 475 Brannan St., San Francisco, CA 94107. Phone: (415) 600-1745. Fax: (415) 600-1725. E-mail: ginesi@cpmcri.com.

[1]Abbreviations: NMBD, N-terminal metal binding domain; TMBS, transmembrane metal binding site; BCA, bicinchoninic acid; SDS, sodium dodecyl sulfate; NP-40, nonyl phenoxypolyethoxylethanol; DTT, dithiothreitol; HEPES, 4-(2-hydroxyethyl)-1-piperazineethanesulfonic acid; MOPS, 3-(*N*-morpholino)propanesulfonic acid; FBS, fetal bovine serum; DMEM, Dulbecco's modified Eagle's medium; EDTA, ethylenediaminetetraacetic acid; DAPI, 4′,6-diamidino-2-phenylindole; PBS, phosphate-buffered saline.

 Published on Web 10/21/2010 © 2010 American Chemical Society

that may be related to different cell types sustaining expression. We observed significant differences with regard to glycosylation and phosphorylation, as well as trafficking patterns of ATP7A and ATP7B in response to copper load, even though the two proteins were expressed in the same cell type and by identical procedures.

EXPERIMENTAL PROCEDURES

Methods for construction of recombinant adenovirus vectors containing CMV promoter-driven ATP7A or ATP7B cDNA fused with a 3′ c-myc tag (rAdATP7Amyc or rAdATP7Bmyc), infection of COS-1 cells, and immunostaining for detection of the heterologous ATP7A or ATP7B protein, were previously described in detail for ATP7B (*15*). Preparation of the microsomal fraction from infected COS-1 cells was also described previously (*15*).

Total protein determination was achieved via the Pierce BCA assay. SDS gel electrophoresis was performed by the method of Laemmli (*16*) at pH 8.3 or Weber and Osborn (*17*) at pH 6.3. The gels were stained with either Coomassie Blue R-250 (Sigma) for detection of protein bands or Pro-Q Emerald (Invitrogen) for detection of glycoprotein. In addition, the protein was transferred from the gels to a PDVF membrane for Western blotting, which was then visualized using 9E10 monoclonal antibodies against the c-myc tag. In some experiments, before electrophoresis, we subjected the microsomal protein to deglycosylation by dissolving 50 μg of microsomal protein in 40 μL of reaction buffer containing 50 mM sodium phosphate, 0.25% SDS, 20 mM DTT, and protease inhibitor cocktail (Sigma) (pH 7.5). Tergitol-type NP-40 was then added to a final concentration of 1%, followed by 2500 units of endoglycosidase PNGase F (NEB). The mixture was incubated at 37 °C for 4 h. The reaction was stopped via addition of loading buffer, and the samples were subjected to electrophoresis and immunoblotting analysis. A parallel incubation was conducted in the absence of PNGase to serve as a negative control.

Purification of His-tagged ATP7A protein was achieved via solubilizing microsomes (5 mg of protein) with 5 mL of solubilization buffer [20 mM Tris, 150 mM NaCl, 1 mM 2-mercaptoethanol, 20% glycerol, 1% LDS, and protease inhibitor cocktail (Roche) (pH 7.5)], followed by a 15 min incubation at room temperature and centrifugation at 12000 rpm for 5 min (Beckman microfuge). The supernatant was collected and mixed with 1 mL of nickel affinity resin (Qiagen) and shaken for 1 h. Unbound proteins were removed by centrifugation at 2000 rpm for 5 min, and the resin was washed three times with 1 mL of wash buffer [20 mM Tris, 150 mM NaCl, 5 mM imidazole, 1 mM 2-mercaptoethanol, 20% glycerol, and 0.1% LDS (pH 7.5)]. The bound protein was then eluted from the resin with 1 mL of elution buffer [20 mM Tris, 150 mM NaCl, 100 mM imidazole, 1 mM 2-mercaptoethanol, 20% glycerol, and 0.1% LDS (pH 7.5)] and shaken gently for 30 min followed by centrifugation at 2000 rpm for 5 min to eliminate the resin. A second elution step was at times used to collect residual protein bound to the resin. The entire procedure was performed at room temperature.

[^{32}P]Phosphoenzyme formation by utilization of [γ-^{32}P]ATP was achieved via incubation of ATP7A or ATP7B (50 μg of microsomal protein/mL) with 50 μM [γ-^{32}P]ATP at 30 °C, in a reaction mixture containing 50 mM MES triethanolamine (pH 6.0), 300 mM KCl, 10 mM DTT, and 3 mM $MgCl_2$. No copper or various concentrations of $CuCl_2$ or BCS were added, as specified in the figure legends. Samples were quenched at serial times with 5% trichloroacetic acid, pelleted by centrifugation at 5000 rpm for 5 min, resuspended in pH 8.3 or 6.3 loading buffer, and separated by Laemmli (*16*) or Weber−Osborn (*17*) gel electrophoresis. The gels were dried and exposed to a phosphor screen followed by scanning using a Typhoon scanner (Amersham).

In some cases, [^{32}P]phosphoenzyme formation was assessed in microsomes pretreated with λ-protein phosphatase (NEB). The phosphatase treatment was conducted in 100 μL of reaction buffer [2400 units of λ-protein phosphatase, 50 mM HEPES, 100 mM NaCl, 2 mM DTT, 0.01% Brij 35, and 1 mM $MnCl_2$ (pH 7.5)] containing 1 mg of microsomal protein at 30 °C for 30 min. The reaction was stopped by the addition of phosphatase inhibitor cocktail (Sigma). The reaction mixture was diluted to 1 mL with microsome resuspension buffer [0.25 M sucrose and 10 mM MOPS (pH 7.0)], mixed by vortexing, and centrifuged at 14000 rpm for 15 min. The pellet was resuspended in microsome resuspension buffer to a final volume of 200 μL. A parallel incubation was conducted in the absence of λ-protein phosphatase to serve as a negative control.

Immunostaining of COS-1 Cells Sustaining Expression of ATP7A or ATP7B. COS-1 cells were grown in a 60 mm culture dish until they reached 60−70% confluence in DMEM containing 10% FBS, inside a CO_2 incubator at 37 °C. The cells were infected with optimal rAdATP7Bmyc viral titers as determined by preliminary cytotoxicity and expression titrations. Following incubation for 48 or 72 h in a CO_2 incubator, the cells were detached using a 0.25% trypsin-EDTA solution (Invitrogen) and reseeded on a sterile coverslip that was placed in a 35 mm culture dish. Following incubation at 37 °C in the CO_2 incubator for an additional 5 h to obtain a uniform cell distribution, the cells were fixed with 3.7% (v/v) paraformaldehyde in PBS for 20 min, followed by permeabilization with 0.1% Triton X-100 in PBS for 15 min at room temperature. The permeabilized COS-1 cells were blocked with 10% horse serum in PBS for 1 h at room temperature followed by the incubation with the diluted primary anti-myc monoclonal antibody (9E10) at 4 °C overnight in block solution. The primary antibodies were detected by incubation of the cells with anti-mouse Alexa 488-conjugated antibodies (Invitrogen) diluted (1:200) in the block solution for 2 h at room temperature. The nuclei of the infected cells were stained with propidium iodide or DAPI. Each step was followed by three rinses with PBS. Finally, the stained cells were evaluated for ATP7Bmyc expression using a confocal laser scanning microscope (Nikon, Eclipse TE2000-U).

Co-Immunostaining of the Plasma Membrane and ATP7A Protein. COS-1 cells were infected with optimal rAdATP7Amyc viral titers as explained above, and following incubation for 2 h in a CO_2 incubator, the cells were treated with 200 μM copper, after 24 h fixed with 3.7% (v/v) paraformaldehyde in PBS for 20 min, and permeabilized with 0.1% Triton in PBS for 15 min. The cells were then rinsed two additional times before being incubated in blocking buffer containing 10% horse serum in PBS for 1 h at room temperature and subsequently incubated with the mouse anti-Myc tag primary antibody (9E10) (1:500) and rabbit anti-Pan Cadherin (1:200) diluted in blocking buffer in a humidified chamber overnight at 4 °C. The cells were then washed three times in PBS and then incubated with Alexa Fluor 555 goat anti-rabbit and Alexa Fluor 488 goat anti-mouse secondary antibodies (diluted 1:500 in blocking buffer) for 1 h at room temperature in the dark. The coverslips were washed and mounted in mounting medium with either DAPI or propidium iodide before confocal scanning (Nikon, Eclipse TE2000-U).

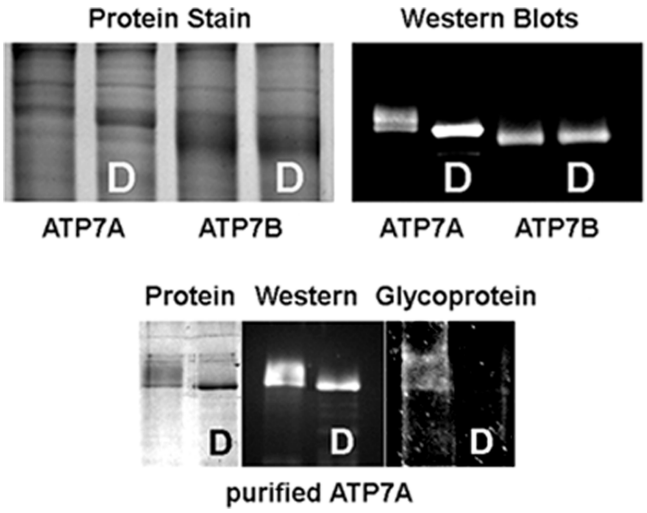

FIGURE 1: Electrophoretic analysis of microsomal proteins derived from COS-1 cells expressing ATP7A or ATP7B and purified ATP7A protein. Protein stain was obtained with Coomassie Blue R-250; glycoprotein stain was obtained with Prop_Q Emerald 300, and Western blots were obtained with 9E10 monoclonal antibodies against the c-myc tag in the expressed protein. D denotes samples subjected to deglycosylation before electrophoresis.

RESULTS

Characterization in the Microsomal Fraction of COS-1 Cells Sustaining Expression of ATP7A or ATP7B. Similar levels of ATP7A and ATP7B proteins are shown by electrophoretic analysis of microsomal fractions obtained from COS-1 cells sustaining heterologous expression. However, the ATP7A protein appears as a diffuse band, while ATP7B appears as a sharp band, as evidenced by protein staining or by immunostaining of the c-myc tag present in both proteins (Figure 1, top panel). If the microsomal proteins are subjected to digestion with glycosidase before electrophoresis, the ATP7A protein runs as a single and sharp band that is smaller, while the mobility of the ATP7B band is not affected at all (Figure 1, top panel). We then purified the ATP7A, taking advantage of a His tag placed in the expression construct, and obtained a much better demonstration of glycosylation (Figure 1, bottom panel). In fact, even the purified protein exhibits an extended band on protein stain, Western blots, and glycoprotein staining. Following deglycosylation, the ATP7A band becomes compact on protein-stained and Western-blotted gels and disappears in the glycoprotein-stained gel. The rather wide appearance of the ATP7A before incubation with glycosidase is likely due to uneven levels of maturity and glycosylation of the nascent protein at the time of harvesting.

Phosphorylation Reactions following Utilization of ATP by the Microsomal Fraction of COS-1 Cells Sustaining Expression of ATP7A or ATP7B. Incubation of microsomal fractions with [γ-^{32}P]ATP, quenched at serial times with trichloroacetic acid, results in phosphorylation of ATP7A and ATP7B, yielding [γ-^{32}P]phosphoprotein that can be visualized by gel electrophoresis. As previously reported for ATP7B (*15*), the resulting [γ-^{32}P]phosphoprotein includes an alkali labile component and an alkali stable component, clearly distinguished by solubilization and electrophoresis of the quenched product in acid (*17*) or alkaline (*16*) buffer. We find that the alkali stable component is much less prominent for ATP7A than for ATP7B (Figure 2). In addition, as observed by immunostaining (Figure 1), the ATP7A [γ-^{32}P]phosphoprotein band is rather wide, as compared with the sharp ATP7B [γ-^{32}P]phosphoprotein band (Figure 2). In analogy with ATP7B (*15*), formation of both the prominent alkali labile and the minor alkali stable phosphoprotein of ATP7A is copper-dependent (Figure 3).

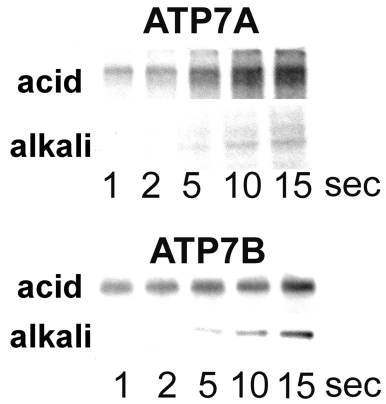

FIGURE 2: Phosphorimaging of electrophoretic gels loaded with ATP7A or ATP7B [^{32}P]phosphoprotein. The proteins were reacted with [γ-^{32}P]ATP at 30 °C to follow formation of phosphoprotein as a function of time. The reaction was stopped with trichloroacetic acid at sequential times as indicated, and the quenched samples were dissolved in detergent at acidic or alkaline pH and separated by electrophoresis at acidic or alkaline pH. Note that the band intensity is much more intense when the electrophoresis is run at acidic as compared to alkaline pH, and the residual alkali resistant phosphoprotein is more intense for ATP7B than for ATP7A.

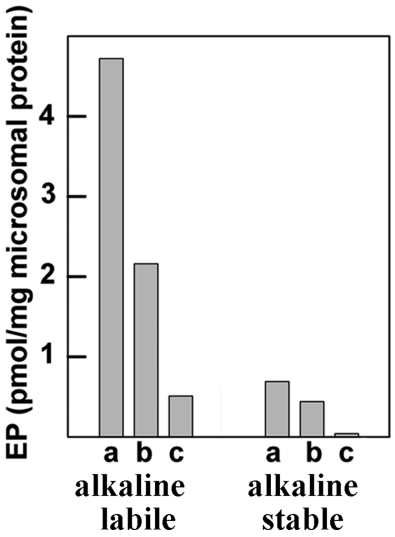

FIGURE 3: Copper dependence of ATP7A phosphorylation. Incubation of microsomes (derived from COS-1 cells sustaining ATP7A expression) with [γ-^{32}P]ATP was allowed to proceed for 10 s at 30 °C, in the presence of 5 μM added $CuCl_2$, no copper, or 5 mM BCS. The columns show the alkali labile and alkali stable phosphoprotein levels obtained in the presence of 5 μM $CuCl_2$ (a), no added (b), and 5 mM copper chelator BCS (c).

Formation of the Phosphoenzyme Intermediate. The alkaline labile portion of the ATP7A and ATP7B phosphoprotein is attributed to phosphorylation of the invariant aspartyl residue of P-type ATPases, yielding the catalytic intermediate of the ATPase cycle. In fact, we found that alkali labile phosphoenzyme is not formed following mutation of the invariant aspartate (*15*). It is apparent from Figure 4 that formation of alkaline labile phosphoprotein (i.e., aspartate phosphorylation) is faster than formation of alkali stable phosphoprotein (i.e., serine phosphorylation) and reaches near maximal levels within 1 or 2 s

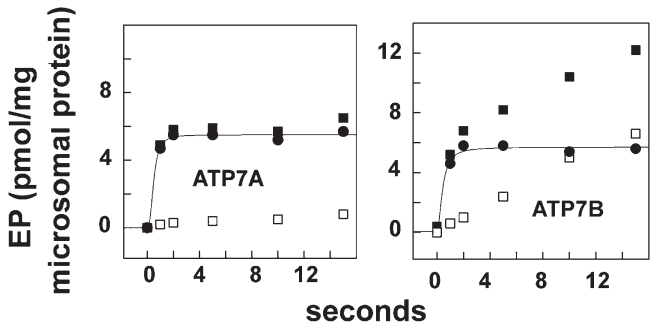

FIGURE 4: Time course of ATP7A and ATP7B phosphoenzyme formation. Microsomes obtained from COS-1 cells sustaining expression of ATP7A or ATP7B were reacted with [γ-^{32}P]ATP at 30 °C for sequential times as indicated, to follow formation of [γ-^{32}P]phosphoprotein as a function of time (see Experimental Procedures). Following acid quenching at sequential times, the quenched samples were dissolved in detergent at acidic or alkaline pH and separated by electrophoresis at acidic or alkaline pH. The data show results obtained with acidic medium electrophoresis (■), alkaline medium electrophoresis (□), and net alkali labile phosphoprotein (i.e., phosphoenzyme intermediate) (●). Note that in all cases the alkaline stable phosphorylation (serines) occurs at a lower rate than the alkaline labile phosphorylation (aspartate) and is more prominent for ATP7B than for ATP7A.

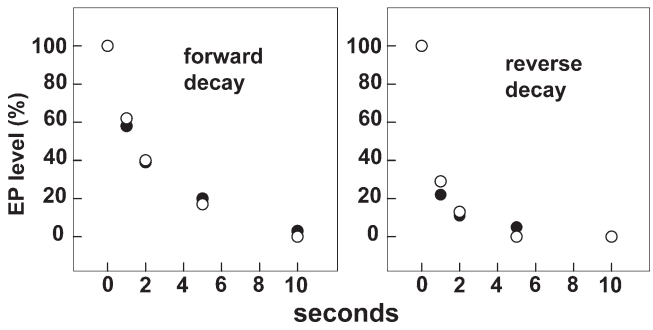

FIGURE 5: Decay of the phosphorylated enzyme intermediate in the forward and reverse direction of the catalytic cycle. Microsomes obtained from COS-1 cells sustaining expression of ATP7A (●) or ATP7B (○) were reacted with [γ-^{32}P]ATP at 10 °C for 15 s, at which time 1 mM nonradioactive ATP or ADP was added, and the samples were acid quenched at various times as indicated. The quenched samples were dissolved in detergent at acidic or alkaline pH and separated by electrophoresis at acidic or alkaline pH. The figure displays residual acid labile [^{32}P]phosphoprotein (i.e., phosphorylated enzyme intermediate) following addition of nonradioactive ATP (forward direction of the cycle) or ADP (reverse direction of the cycle).

at 30 °C. To compare the turnover of the ATP7A and ATP7B [^{32}P]phosphoenzyme intermediate, we performed a chase with nonradioactive ATP and obtained satisfactory time resolution at 10 °C. We found that for both ATP7A and ATP7B the [^{32}P]phosphoenzyme intermediate decays with a half-time of approximately 2 s (Figure 5, left panel), corresponding to forward turnover.

It should be pointed out that faster kinetics for ATP7A than ATP7B were previously reported (*18*). However, the reported kinetics were on the minute time scale, as opposed to our second time scale (Figure 4). In addition, using the same type of ATP7B expression, no serine phosphorylation was observed (*6*), as demonstrated following aspartate mutation. It is possible that expression in insect cells (*6*, *18*) does not include post-translational modifications that are required for correct folding and adequate function of the protein. Our expression in mammalian

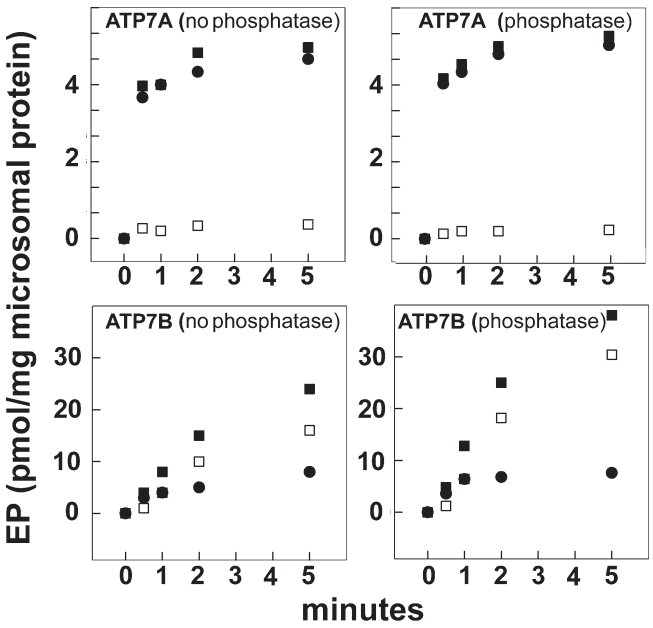

FIGURE 6: Effect of preincubation with λ-protein phosphatase on the levels of ATP7A and ATP7B [γ-^{32}P]phosphoprotein formed by utilization of ATP. Microsomes obtained from COS-1 cells sustaining expression of ATP7A or ATP7B were incubated for 30 min at 30 °C, in the presence or absence of λ-protein phosphatase (see Experimental Procedures). Following centrifugation and resuspension, the microsomal protein (50 μg/mL) was incubated with 50 μM [γ-^{32}P]ATP at 30 °C, as explained in Experimental Procedures. The quenched samples were dissolved in detergent at acidic or alkaline pH and separated by electrophoresis at acidic or alkaline pH.

cells yields kinetics on the second time scale (as expected of an enzyme), allows serine phosphorylation of ATP7B, and exhibits a stoichiometry compatible with the expressed protein.

We also observed that decay of [γ-^{32}P]phosphoenzyme intermediate formation following a chase with nonradioactive ADP, corresponding to reverse turnover, is significantly faster (Figure 5, right panel). This indicates that the observed [^{32}P]phosphoenzyme includes mostly the first intermediate in the P-ATPase cycle (E1-P), before the rate-limiting transition to the conformational isomer (E2-P) that then undergoes hydrolytic cleavage.

Alkali Stable Phosphoprotein. The residual phosphoprotein revealed by electrophoresis at alkaline pH (alkali stable) is related to phosphorylation of serine residues, as demonstrated by mass spectrometry (*15*). Considering that the alkali resistant phosphoprotein level is lower for ATP7A than for ATP7B (Figures 3 and 4), we wondered whether phosphorylation of serines ex vivo (in the cultured cells sustaining expression) may have limited the number of serines available for phosphorylation in vitro. To clarify this uncertainty, we preincubated microsomes containing ATP7A or ATP7B for 30 min at 30 °C in the presence or absence of λ-protein phosphatase before performing phosphorylation experiments with [γ-^{32}P]ATP in vitro. We found that cleavage of the phosphoenzyme formed ex vivo did in fact result in increased levels of alkali resistant ATP7B phosphorylation in vitro [from 13 to 24 pmol/mg of microsomal protein produced in 5 min (Figure 6)]. On the other hand, alkali resistant phosphorylation of ATP7A occurred at a similarly low level [0.4−0.5 pmol/mg of microsomal protein produced in 5 min (Figure 6)], with and without prior incubation with λ-protein phosphatase. These results clearly show that the level of serine phosphorylation is lower in ATP7A than in ATP7B. On the other hand, it is important to note that alkali labile phosphorylation (i.e., phosphoenzyme

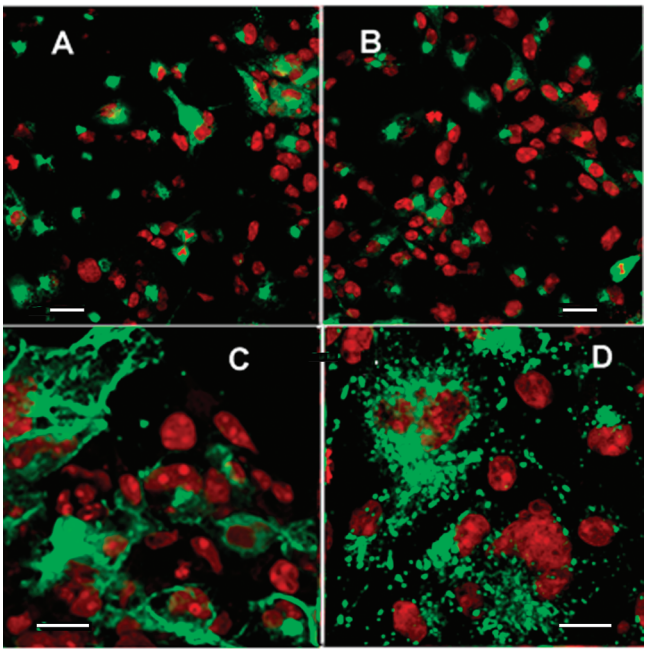

FIGURE 7: Cytosolic distribution of ATP7A and ATP7B in COS-1 cells following infection with viral vector in the presence of basal or added $CuCl_2$. COS-1 cells were infected with optimal rAdATP7Amyc or rAdATP7Bmyc viral titers as explained in Experimental Procedures. ATP7A (A and C) and ATP7B (B and D) were immunostained with the primary anti-myc tag monoclonal antibody and anti-mouse Alexa 488 secondary antibody (colored green). The nuclei are stained with propidium iodide (colored red). It is shown that, in the absence of added copper, the expressed ATP7A (A) and ATP7B (B) proteins (green) are mostly visible near the nuclei (red color), corresponding to the Golgi and trans-Golgi network. In the presence of added copper, ATP7A (C) is partly retained near the nuclei and partly targeted to plasma membranes; no trafficking vesicles are observed. On the other hand, ATP7B (D) is associated with numerous trafficking vesicles throughout the cytoplasm, with no significant plasma membrane association. The bar is 10 μm.

intermediate) reaches approximately the same levels (4−5 nmol/mg of microsomal protein) in ATP7B and ATP7A, in a manner independent of preincubation with λ-protein phosphatase (Figures 4 and 6).

Trafficking Patterns of ATP7A and ATP7B Expressed in COS-1 Cells. An important feature of ATP7A and ATP7B is their copper responsive trafficking (*19*, *20*). To determine whether intrinsic features of ATP7A or ATP7B expressed in the same cell type may contribute to different trafficking patterns, we examined by immunostaining COS-1 cells sustaining heterologous expression of either protein. We found that, in the absence of added copper (Figure 7A,B), both proteins (green in Figure 7) were located near the nuclei (red in Figure 7), corresponding to the Golgi and trans-Golgi network. When the cells were subjected to a copper load, a significant portion of the ATP7A protein was shifted to peripheral membranes (Figure 7C), while following the same copper load, a prevalent fraction of the ATP7B protein joined numerous trafficking vesicles in the cytoplasm (Figure 7D). We then performed additional experiments to obtain microscopic images with greater resolution and found that ATP7A, identified by immunostaining with an anti-myc tag antibody (green in Figure 8A), is predominantly localized on plasma membranes identified by immunostaining with anti-Pan Cadherin antibody (red in Figure 8B). Colocalization in the plasma membrane is further demonstrated by an overlay (Figure 8D). The clearly different trafficking patterns of ATP7A and ATP7B were observed in experiments performed several times in parallel, using COS-1 cells infected with the same viral titers, and maintained under the same conditions.

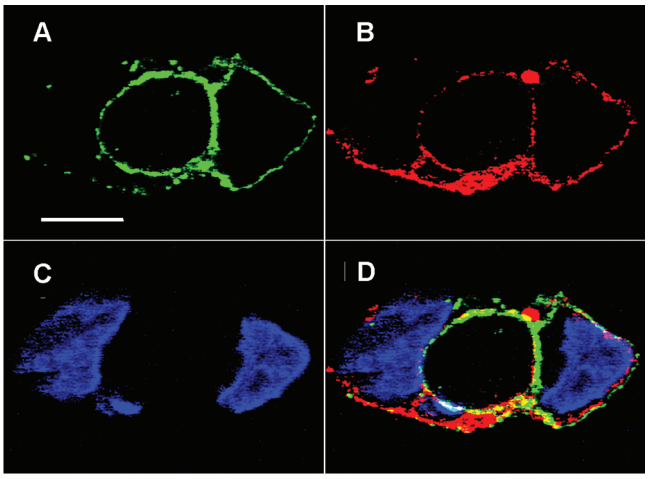

FIGURE 8: Association of ATP7A protein with the plasma membrane of COS-1 cells. COS-1 cells were infected with optimal rAdATP7Amyc viral titers as explained in Experimental Procedures, and 200 μM copper was added. After 24 h, the cells were fixed with paraformaldehyde, permeabilized with Triton X-100, and stained (see Experimental Procedures). Immunostaining of ATP7A with the anti-myc tag antibody is shown in green (A), and plasma membrane immunostaining with the anti-Pan Cadherin antibody is shown in red (B). Nuclear staining with DAPI is shown in blue (C). The overlay in panel C demonstrates colocalization of ATP7A and anti-Pan Cadherin antibodies in the plasma membrane. The bar is 10 μm.

DISCUSSION

ATP7A and ATP7B are both copper-activated P-type ATPases involved in copper acquisition, delivery of copper to metalloproteins in the secretory pathway, and export of excess copper from cells. It is clear that a catalytically active conformational state of both proteins is important for membrane trafficking and copper transport (*1*). In fact, in our experiments, the catalytic properties of the two enzymes, including activation by copper, a phosphorylated intermediate, and kinetic turnover, are quite similar (Figures 4 and 5). On the other hand, specific features of ATP7A and ATP7B are revealed by the diverse phenotypes of diseases related to defects of either gene. Furthermore, while ATP7A appears to be involved in trafficking to the basolateral membrane of polarized cells, ATP7B is engaged in export of copper but also in the delivery of copper to the secretory pathways (*1*). These specific patterns are likely related, at least in part, to specific features of different cell types. On the other hand, in our experiments, expression of ATP7A and ATP7B in the same mammalian cell type allowed a comparative evaluation of intrinsic features of the two proteins. In fact, we observed differences in post-translational modifications, inasmuch as ATP7A undergoes glycosylation, while ATP7B does not (Figure 2). Furthermore, ATP7A undergoes a much lower level of alkali stable (serine) phosphorylation than ATP7B (Figures 4 and 6).

The difference in glycosylation is consistent with protein sequence analysis (Table 1) revealing several glycosylation motifs in ATP7A, including N686MS and N975RS within the cytosolic loops between transmembrane segments 1 and 3 and segments 5 and 6. These loops are expected to acquire extracellular exposure upon plasma membrane localization of the ATP7A protein. As originally shown by Katz et al. (*21*), newly synthesized and glycosylated proteins are assembled asymmetrically on rough

Table 1: ATP7A (**7A**) Sequence Segments, Including Glycosylation Motifs (bold and underlined) and ATP (**7B**) Sequence Segments Aligned with the Corresponding ATP7B Segments[a]

```
7A  MDPSMGVNSVTISVEGMTCNSCVWTIEQQIGKVNGVHHIKVSLEEKNATIIYDPKLQTPK 60
7B  ----------------------MPEQERQITAREGASRKILSKLS-LPTRAWEPAMKK-- 35
                          :   *:**   :*. :  :*  .  .*  ::* ::.

7A  QPKYLKLGAIDVERLKNT----PVKSSEGSQQRSPSYTNDS----TATFIIDGMHCKSCV 292
7B  KVAPLSLGPIDIERLQSTNPKRPLSSANQNFNNSETLGHQGSHVVTLQLRIDGMHCKSCV 272
    :   *.**.**:***:.*    *:.*:: . :.* :  ::.    *  : **********

7A  SNIESTLSALQYVSSIVVSLENRSAIVKYNASSVTPESLRKAIEAVSPGLYRVSITSEVE 352
7B  LNIEENIGQLLGVQSIQVSLENKTAQVKYDPSCTSPVALQRAIEALPPGNFKVSLPDGAE 332
     ***..:. *  *.** *****::* ***:.*..:* :*::****:.** ::**:.. .*

7A  SLANSNGTVEYDPLLTSPETLRGAIEDMGFDATLSDTNEPLVVIAQPSSEMPLLTSTN-- 468
7B  SLAEGTATVLYNPSVISPEELRAAIEDMGFEASVVSESCSTNPLGNHSAGNSMVQTTDGT 452
    ***:...** *:* : *** **.*******:*:: . . .   :.: *:  .:: :*:

7A  KKDRSASHLDHKREIRQWRRSFLVSLFFCIPVMGLMIYMMVMDHHFATLHHNQNMSKEEM 692
7B  QRNPNAHHLDHKMEIKQWKKSFLCSLVFGIPVMALMIYMLIPSN---------------- 676
    ::: .* ***** **:**::*** **.* ****.*****:: .:

7A  LITGEAMPVAKKPGSTVIAGSINQNGSLLICATHVGADTTLSQIVKLVEEAQTSKAPIQQ 932
7B  LITGEAMPVTKKPGSTVIAGSINAHGSVLIKATHVGNDTTLAQIVKLVEEAQMSKAPIQQ 915
    *********:************* :**:** ***** ****:********** *******

7A  FADKLSGYFVPFIVFVSIATLLVWIVIGFLNFEIVETYFPGYNRSISRTETIIRFAFQAS 992
7B  LADRFSGYFVPFIIIMSTLTLVVWIVIGFIDFGVVQRYFPNPNKHISQTEVIIRFAFQTS 975
    :**::********:::*  **:*******::* :*: ***. *: **:**.*******:*

7A  PTYESYELPARSQIGQKSPSEISVHVGIDDTSRNSPKLGLLDRIVNYSRASINSLLSDKR 1472
7B  PDLERYEAQAHGHMKPLTASQVSVHIGMDDRWRDSPRATPWDQVSYVSQVSLSSLTSDKP 1438
    *  * **  *:.::   :.*::***:*:**  *:**:    *::   *:.*:.** ***
```

[a]Asterisks denote identical residues, colons conserved substitutions, and periods semiconserved substitutions (Clustal W).

endoplasmic reticulum membranes and then migrate and fuse with the plasma membrane by exocytosis, resulting in protein membrane assembly and stabilization. This would explain the ATP7A membrane association observed in our experiments (Figure 8). On the other hand, no glycosylation sites are noted in the ATP7B sequence, with the exception of Asn_{303}AsnSer and

Asn_{353}LeuThr within the NMBD, predicted to face the cytosol upon insertion of the protein in the plasma membrane. Glycosylation of ATP7A was originally implied in studies by Yamaguchi et al. (*22*).

In our experiments for expression in COS-1 cells, we found that phosphorylation of serine residues ("alkaline resistant phosphorylation") is more prominent in ATP7B than in ATP7A (Figures 2, 4, and 6). This is again consistent with sequence analysis, considering that of the serine residues (Ser478, Ser481, Ser1121, and Ser1453) shown to undergo phosphorylation in ATP7B (*15*), only Ser1486 (corresponding to Ser1453 of ATP7B) is present in the ATP7A sequence. Phosphorylation of serine residues is likely to play an important role in copper ATPase's regulation and trafficking (*23*), and in our experiments, the high level of serine phosphorylation may account for the high density of ATP7B associated with trafficking vesicles in the cytoplasm of cells subjected to a copper load (Figure 7D). It is well-known that phosphorylation is involved in regulation and localization of membrane-bound proteins (*24*, *25*). Phosphorylation of Thr947 in the carboxyl terminus of another P-type ATPase (plasma membrane H^+-ATPase AHA2) is required for high-affinity binding of regulatory proteins (*26*). It may be relevant that in ATP7B, Ser1453 is followed by a unique COOH terminus three-leucine zipper motif (only two leucines follow Ser1486 of ATP7A), which is known to play a role in scaffolding and receptor targeting (*27*).

In conclusion, our experiments indicate that the catalytic properties of ATP7A and ATP7B, including intermediate formation and turnover of the phosphorylated aspartyl residue, are quite similar. However, different levels of glycosylation and serine phosphorylation are likely to contribute to specific trafficking patterns and membrane targeting of ATP7A and ATP7B, observed when the two proteins are expressed in the same mammalian cell type.

REFERENCES

1. Lutsenko, S., Barnes, N. L., Bartee, M. Y., and Dmitriev, O. Y. (2007) Function and regulation of human copper-transporting ATPases. *Physiol. Rev. 87*, 1011–1046.
2. Lutsenko, S., and Kaplan, J. H. (1995) Organization of P-type ATPases: Significance of structural diversity. *Biochemistry 34*, 15607–15613.
3. Burroughs, A. M., Allen, K. N., Dunaway-Mariano, D., and Aravind, L. (2006) Evolutionary genomics of the HAD superfamily: Understanding the structural adaptations and catalytic diversity in a superfamily of phosphoesterases and allied enzymes. *J. Mol. Biol. 361*, 1003–1034.
4. Banci, L., Bertini, I., Cantini, F., Massagni, C., and Migliardi, M. (2009) An NMR study of the interaction of the N-terminal cytoplasmic tail of the Wilson disease protein with copper(I)-HAH1. *J. Biol. Chem. 284*, 9354–9360.
5. Leshane, E. S., Shinde, U., Walker, J. M., Barry, A. N., Blackburn, N. J., Ralle, M., and Lutsenko, S. (2010) Interactions between copper-binding sites determine the redox status and conformation of the regulatory N-terminal domain of ATP7B. *J. Biol. Chem. 285*, 6327–6336.
6. Tsivkovskii, R., Eisses, J. F., Kaplan, J. H., and Lutsenko, S. (2002) Functional properties of the copper-transporting ATPase ATP7B (the Wilson's disease protein) expressed in insect cells. *J. Biol. Chem. 277*, 976–983.
7. Hung, Y. H., Layton, M. J., Voskoboinik, I., Mercer, J. F., and Camakaris, J. (2007) Purification and membrane reconstitution of catalytically active Menkes copper-transporting P-type ATPase (MNK; ATP7A). *Biochem. J. 401*, 569–579.
8. Linz, R., and Lutsenko, S. (2007) Copper-transporting ATPases ATP7A and ATP7B: Cousins, not twins. *J. Bioenerg. Biomembr. 39*, 403–407.
9. Monty, J. F., Llanos, R. M., Mercer, J. F., and Kramer, D. R. (2005) Copper exposure induces trafficking of the menkes protein in intestinal epithelium of ATP7A transgenic mice. *J. Nutr. 135*, 2762–2766.
10. Greenough, M., Pase, L., Voskoboinik, I., Petris, M. J., O'Brien, A. W., and Camakaris, J. (2004) Signals regulating trafficking of Menkes (MNK; ATP7A) copper-translocating P-type ATPase in polarized MDCK cells. *Am. J. Physiol. 287*, C1463–C1471.
11. Weiss, K. H., Lozoya, J. C., Tuma, S., Gotthardt, D., Reichert, J., Ehehalt, R., Stremmel, W., and Füllekrug, J. (2008) Copper-induced translocation of the Wilson disease protein ATP7B independent of Murr1/COMMD1 and Rab7. *Am. J. Pathol. 173*, 1783–1794.
12. Roelofsen, H., Wolters, H., Van Luyn, M. J., Miura, N., Kuipers, F., and Vonk, R. J. (2000) Copper-induced apical trafficking of ATP7B in polarized hepatoma cells provides a mechanism for biliary copper excretion. *Gastroenterology 119*, 782–793.
13. Barnes, N., Bartee, M. Y., Braiterman, L., Gupta, A., Ustiyan, V., Zuzel, V., Kaplan, J. H., Hubbard, A. L., and Lutsenko, S. (2009) Cell-specific trafficking suggests a new role for renal ATP7B in the intracellular copper storage. *Traffic 10*, 767–779.
14. Gupta, A., and Lutsenko, S. (2009) Human copper transporters: Mechanism, role in human diseases and therapeutic potential. *Future Med. Chem. 1*, 1125–1142.
15. Pilankatta, R., Lewis, D., Adams, C. M., and Inesi, G. (2009) High yield heterologous expression of wild-type and mutant Cu^+-ATPase (ATP7B, Wilson disease protein) for functional characterization of catalytic activity and serine residues undergoing copper-dependent phosphorylation. *J. Biol. Chem. 284*, 21307–21316.
16. Laemmli, U. K. (1970) Cleavage of structural proteins during the assembly of the head of bacteriophage T4. *Nature 227*, 680–685.
17. Weber, K., and Osborn, M. (1969) The Reliability of Molecular Weight Determinations by Dodecyl Sulfate-Polyacrylamide Gel Electrophoresis. *J. Biol. Chem. 244*, 4406–4412.
18. Barnes, N., Tsivkovskii, R., Tsivkovskaia, N., and Lutsenko, S. (2005) The copper-transporting ATPases, Menkes and Wilson disease proteins, have distinct roles in adult and developing cerebellum. *J. Biol. Chem. 280*, 9640–9645.
19. La Fontaine, S. L., Firth, S. D., Camakaris, J., Englezou, A., Theophilos, M. B., Petris, M. J., Howie, M., Lockhart, P. J., Greenough, M., Brooks, H., Reddel, R. R., and Mercer, J. F. (1998) Correction of the copper transport defect of Menkes patient fibroblasts by expression of the Menkes and Wilson ATPases. *J. Biol. Chem. 273*, 31375–31380.
20. Veldhuis, N. A., Gaeth, A. P., Pearson, R. B., Gabriel, K., and Camakaris, J. (2009) The multi-layered regulation of copper translocating P-type ATPases. *BioMetals 22*, 177–190.
21. Katz, F. N., Rothamn, J. E., Lingappa, V. R., Blobel, G., and Lodish, H. F. (1977) Membrane Assembly in vitro: Synthesis, glycosylation, and asymmetric insertion of transmembrane protein. *J. Biol. Chem. 74*, 3278–3282.
22. Yamaguchi, Y., Heiny, M. E., Suzuki, M., and Gitlin, J. D. (1996) Biochemical characterization and intracellular localization of the Menkes disease protein. *Proc. Natl. Acad. Sci. U.S.A. 93*, 14030–14035.
23. Lutsenko, S., Gupta, A., Burkhead, J. L., and Zuzel, V. (2008) Cellular multitasking: The dual role of human Cu-ATPases in cofactor delivery and intracellular copper balance. *Arch. Biochem. Biophys. 476*, 22–32.
24. Gadsby, D. C., and Nairn, A. C. (1999) Regulation of CFTR Cl^- ion channels by phosphorylation and dephosphorylation. In Ion Channel Regulation. *Physiol. Rev. 79*, S77–S107.
25. Guggino, W. B., and Stanton, B. A. (2006) New insights into cystic fibrosis: Molecular switches that regulate CFTR. *Nat. Rev. Mol. Cell Biol. 7*, 426–436.
26. Fuglsang, A. T., Visconti, S., Dromm, K., Jahn, T., Stensballe, A., Mattei, B., Jensen, O. N., Aducci, P., and Palmgren, M. G. (1999) Binding of 14-3-3 Protein to Plasma Membrane H^+ATPase AHA2 Involves the Three C-terminal Residues Tyr9456-Thr-Val and require phosphorylation of Thr947. *J. Biol. Chem. 274*, 36774–36780.
27. Tadokoro, S., Tachibana, T., Imanaka, T., Nishida, W., and Sobue, K. (1999) Involvement of unique leucine-zipper motif of PSD-Zip45 (Homer 1c/vesl-1L) in group 1 metabotropic glutamate receptor clustering. *Proc. Natl. Acad. Sci. U.S.A. 96*, 13801–13806.